Experimental and numerical investigations on the positive slopes on the pump performance curve of a low specific speed model pump-turbine

G C Lu, Z G Zuo, Y K Sun and S H Liu

Department of Thermal Engineering, Tsinghua University, Beijing, 100084, China

Email: liushuhong@mail.tsinghua.edu.cn

Abstract. The positive slope on the pump performance curve of pump-turbines suggested potential operational instabilities in pump mode. In the present study a low specific speed model pump-turbine was experimentally and numerically examined. The results revealed that the positive slope region exists on each Guide Vane Opening (GVO) curve except at the optimum GVO. The positive slope occurred in the discharge coefficient between 80%-85% optimum discharge coefficient at every GVO. Hysteresis was detected on the occurrence of the positive slope between measurements with increasing and decreasing discharge coefficient. FFT (Fast Fourier Transformation) analysis on pressure fluctuations revealed the occurrence of rotating stall with two cells close to the vaneless space between the runner and the guide vanes in the positive slope region. Two-dimensional simulation was then applied for a further understanding of the flow mechanism of the rotating stall.

1. Introduction

Hydropower pumped storage is widely utilized in commercial as grid-scale energy storage technology. Water is pumped to an upper storage reservoir by pump-turbine when the power supply is higher than the demand, while it is reversed to generate hydroelectric power when the supply is lower than the demand. In the 1960s the pumped storage power stations (PSPS) developed rapidly to the complement the applications of nuclear power [1]. This technology has been used extensively recently for the increasingly renewable-based electricity supply systems, for the benefits of load-levelling, grid frequency regulation, and spinning reserves [2].

Positive slopes can often be observed on the performance curves of pump-turbines in pump mode, which may result in operational instabilities, accompanied with severe noise and vibration. The flow mechanisms of this phenomenon in a pumping system are extraordinarily complex. Gülich [3] summarized them as the "sudden change" of flow patterns at the entrance or exit of the pump impeller. In pump-turbines, diverse flow pattern changes, including rotating stall [4, 5], flow separation shift [6, 7] and pre-rotation of inflow [6], have been reported when pump-turbines operate in the positive slope region.

In the present study, the pump performance of a low specific speed pump-turbine was experimentally investigated. The pressure fluctuations in the draft tube, the vaneless space and the stay vanes channels were measured and analyzed by fast Fourier Transformation (FFT) to detect the flow pattern responsible for the positive slope. For the purpose of a further understanding to the flow mechanism of this flow pattern, two-dimensional simulations were then carried out.

2. Experimental set-up

Experimental investigation was applied on a low specific speed ($n_q = \frac{n\sqrt{Q}}{H^{0.75}} = 27$, where *n*, *Q* represent the rotating speed and the flow rate respectively) model pump-turbine (figure 1), on the *DF150 Hydraulic Test Rig* (figure 2) of Dongfang Electric Corporation (DEC), China. The geometric and operational parameters of the model pump-turbine are listed in table 1, while the operational parameters of this test rig are listed in table 2.

Dynamic miniature piezoelectric pressure sensors (0-345kPa, minimum response frequency 0.5Hz) were flush-mounted on the walls of the draft tube, the vaneless space and the stay vanes channel, in accordance with the IEC standard [8], as illustrated in figure 3.

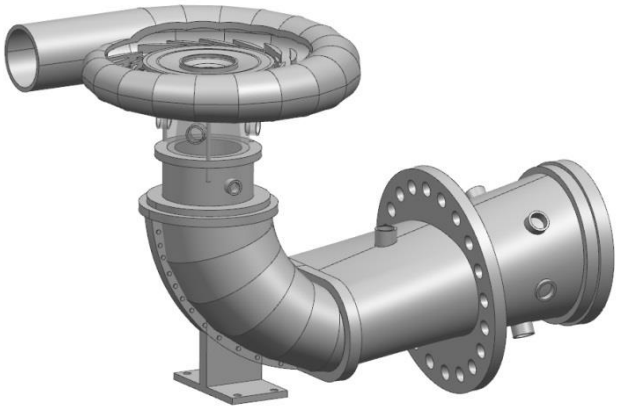

Figure 1. Low specific speed model pump-turbine

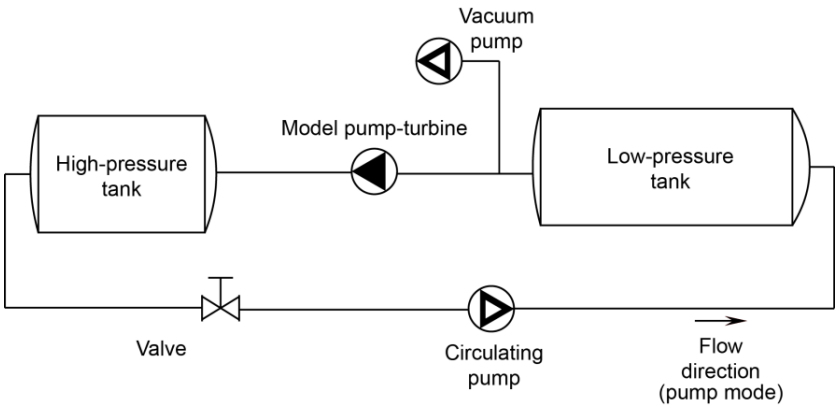

Figure 2. Schematic of *DF150 Hydraulic Test Rig*

Table 1. Geometric and operational parameters of the model pump-turbine

Parameter	Value
Wrap angle of blades (°)	154
Number of blades	7
Impeller inlet diameter (mm)	150
Impeller outlet diameter (mm)	280
Number of guide vanes	20
Height of guide vanes (mm)	37.75
Rotating speed (r/min)	1100

Table 2. Operational parameters of *DF150test rig*

Parameters	Value
Maximum flow rate (m^3/s)	1.5
Maximum head (m)	150
Maximum rotating speed (r/min)	2500
Systematic uncertainty on the efficiency measurement (%)	0.25

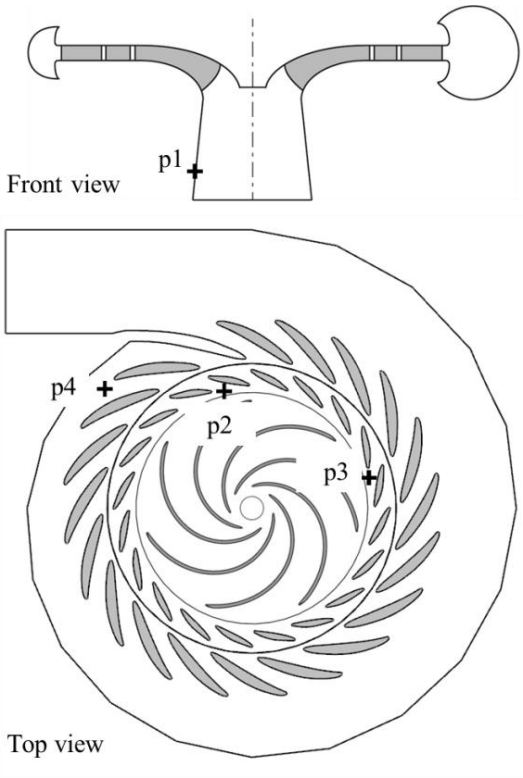

Figure 3. Monitoring points in the draft tube (p1), vaneless space (p2, p3) and stay vane channel (p4)

3. Pump performance

The experimental pump performance curves at different GVOs are shown in figure 4. Here $\varphi=\frac{Q}{nD^3}$ and $\psi=\frac{gH}{n^2D^2}$ represent discharge coefficient and energy coefficient respectively. α represents the ratio of GVO over the optimum GVO (18). The discharge coefficient decreased from high to low when measuring the performance curves. Detailed examination of each curve shows that the positive slope region exists on each GVO curve except at the optimum GVO. Table 3 lists the range of discharge coefficient with positive slope at various GVOs. φ_{min} and φ_{max} represent respectively the minimum and maximum discharge coefficients with positive slope at every GVO, while φ^* indicates the optimum discharge coefficient at this GVO. It could be seen that the positive slope occurs in the discharge coefficient between 80%-85% optimum discharge coefficient at every GVO.

Then the pump performance curves were measured with increasing discharge coefficient. By comparing the pump performance curves between measurements with increasing and decreasing discharge coefficients at three different GVOs (α=145%, 75% and 45%), hysteresis was detected as shown in figure5 (where 'Inc' represents the measurement with an increasing discharge coefficient,

while 'Dec' represents that with a decreasing discharge coefficient). The positive slope still exists but occurs at a smaller discharge coefficient.

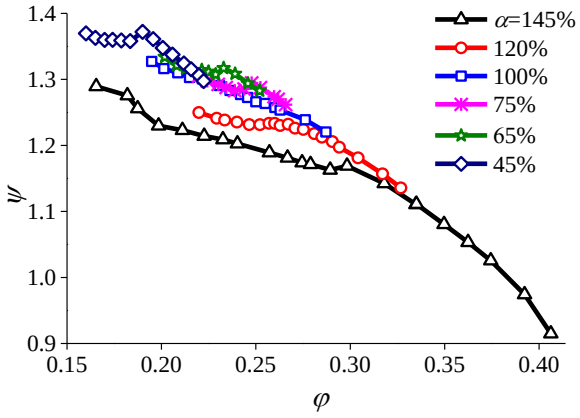

Figure 4. Experimental pump performance curves at various GVOs

Table 3. Range of discharge coefficient with positive slope at various GVOs

α	φ_{min}-φ_{max}	φ^*	φ_{min}/φ^*-φ_{max}/φ^*
145%	0.289-0.298	0.35	82.5%-85%
120%	0.257-0.267	0.317	81.1%-84.2%
75%	0.242-0.254	0.294	82.3%-86.4%
65%	0.229-0.233	0.282	81.2%-82.6%
45%	0.183-0.19	0.225	81.3%-84.4%

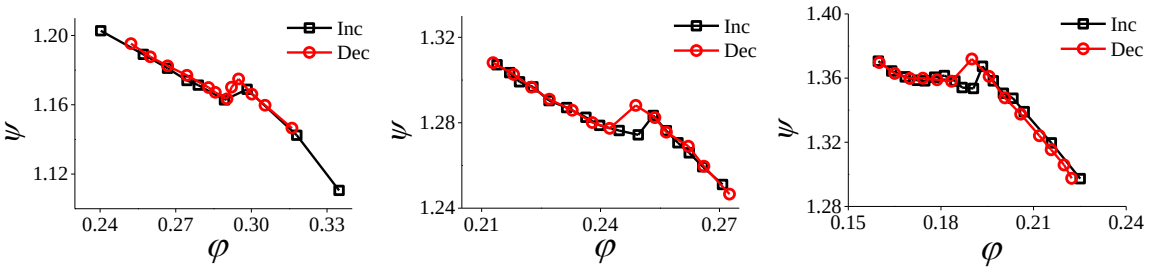

(a) (b) (c)

Figure 5. Pump performance curves when increasing and decreasing discharge coefficient at (a) α=145%, (b) α=75% and (c) α=45%

4. Pressure fluctuations

The measurements of the pressure coefficient ($C_p = \frac{p}{\frac{1}{2}\rho u_2^2}$, where u_2 represents the relative velocity at impeller exit) fluctuations in the draft tube, vaneless space and the stay vane channel at α=45% were applied with decreasing the discharge coefficient and then FFT analysis are shown in figure 6. The dominant frequency of pressure fluctuations is the blade passing frequency (BPF, f_1 in figure 6) at large discharge coefficient, whose amplitude remained almost constant with varying discharge coefficient. The amplitude of BPF component is largest at vaneless space which matches the conclusion in the previous study [9]. When the discharge coefficient decreases into the positive slope region, a pressure fluctuation component with a low frequency (f_2=1.46Hz≈8%f_n in figure 6, where f_n represents the rotating frequency) was detected. Rotating stall may be the flow pattern that is

responsible for this low-frequency fluctuation component, which is stronger at the vaneless space than that at the other two locations, according to previous studies [4, 10]. The cross phase delay of the low-frequency fluctuation component is about 180 degree (figure 7), while the phase difference between the two monitoring points is 90 degree. It implies that two rotating cells exist.

Figure 8 provides a global view of the occurrence of rotating stall by superposing the amplitude of the low-frequency fluctuation component to the pump performance curve. The area of the circles is proportional to the fluctuation amplitude. It could be seen that the amplitude of the low-frequency fluctuation component increases sharply when the discharge coefficient decreased to lower than the maximum discharge coefficient with positive slope, suggesting the possible occurrence of the rotating stall at these working conditions. The situation with increasing the discharge coefficient when measuring is also shown in figure 8. The low-frequency fluctuation component was still detected, when the discharge coefficient is lower than the maximum discharge coefficient with positive slope. Thus, it could be concluded that rotating stall appears when the discharge coefficient decreases to positive slope region, and it disappears when the discharge coefficient increases from positive slope region to negative slope region.

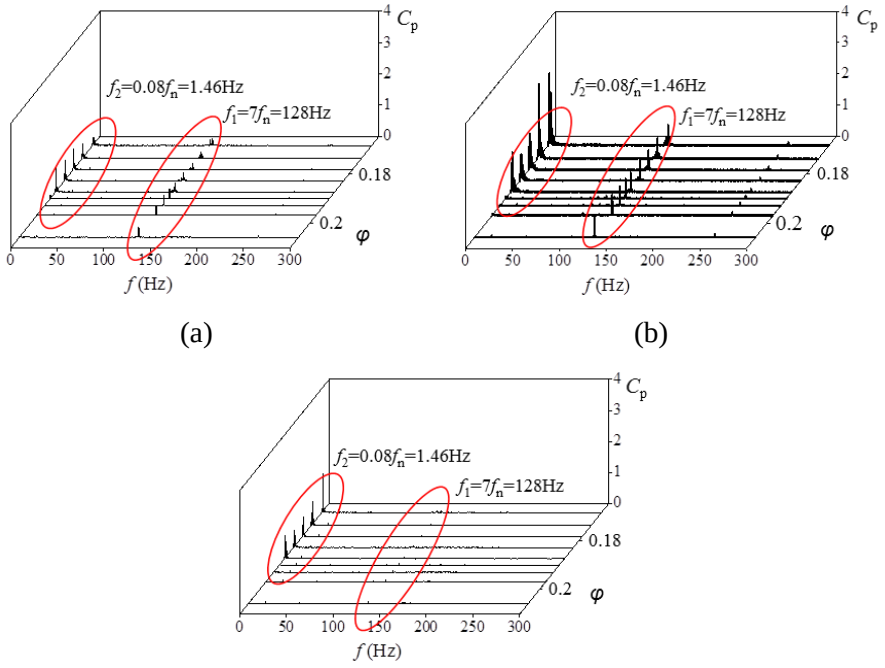

Figure 6. FFT results of pressure fluctuation at (a) stay vane (p1), (b) vaneless space (p2) and (c) draft tube (p4) at α=45%

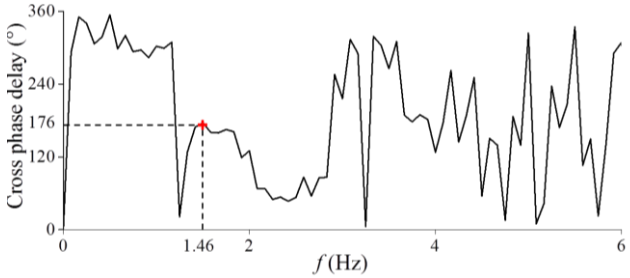

Figure 7. Cross phase delay of the pressure fluctuations between p2 and p3

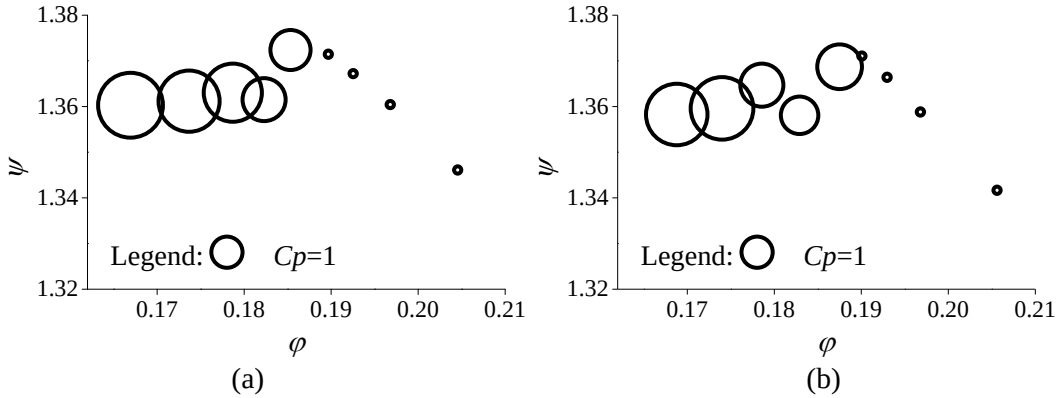

Figure 8. Amplitude of low-frequency fluctuation component at vaneless space(α=45%)with (a) decreasing and (b) increasing discharge coefficient

5. Two-dimensional simulations

Two-dimensional simulation was applied for a further understanding to the flow mechanism of the rotating stall. A computational domain including the fluid channels in the impeller, guide vane (α=145%), stay vane and the spiral casing was built as illustrated in figure 9. The two-dimensional computational domain was simplified from the three-dimensional fluid domain as following:

The impeller component is the projection of S1 surface on the middle section, while the other components are the projections of the corresponding hydraulic components on the middle section. Unsteady numerical simulations based on RANS method with v^2-f turbulence model were applied in commercial software CFX. SIMPLEC was chosen as the pressure-velocity coupling method. The time when the impeller rotates for $1°$ was determined as the computational time step. A structured computational mesh system with almost one million grids for the whole computational domain was developed in ICEM. Local refinements to the boundary layers were applied in the impeller, guide vane and stay vane regions regarding that no wall function is utilized in v^2-f turbulence model, as shown in figure 9. The values of y^+ were compatible with the chosen turbulence model (y^+<10).

The positive slope on the performance curve was detected in the results of the two-dimensional simulations, as shown in figure 10. Here the discharge coefficient is defined as $\varphi = \frac{Q}{nD^3} = \frac{Q_{2D}b}{nD^3}$, where Q_{2D} is the flow rate in the two-dimensional simulation, and b is the width of impeller outlet. The streamlines in the impeller at working conditions P1 and P2 are shown in figure 11. Recirculation was detected at most passages because the inlet area is too small. The flow field in the impeller became strong circumferential asymmetric at the condition with positive slope. Figure 12 shows the pressure distribution in the impeller, guide vane and the stay vane at P1. Four high pressure regions and low pressure regions (cells) distribute alternately in circumferential. Figure 13 illustrates the distribution of velocity and pressure in the guide vane and the stay vane at three different time steps. It could be seen that these high pressure regions and low pressure regions rotate along the rotating direction of impeller, indicating the occurrence of rotating stall. Two channels (C2 and C3) were blocked, and the low pressure region located in C3 when t=0. This low pressure region moved to the location near the guide vane (G4) between C3 and C4 at $t=\frac{1}{30}T$ and then arrived C4 at $t=\frac{1}{15}T$, when C3 and C4 were blocked instead of C2 and C3 at t=0.

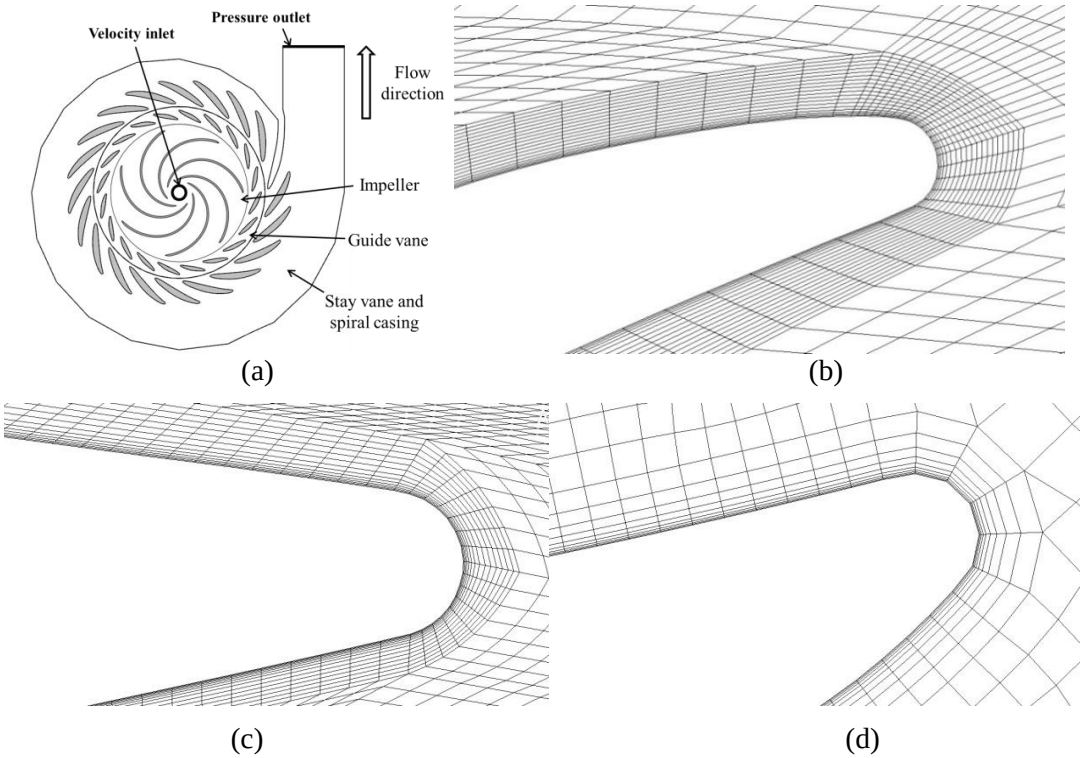

Figure 9. (a) Computational domain and boundary layer grids in (b) impeller, (c) guide vane as well as (d) stay vane for two-dimensional simulations

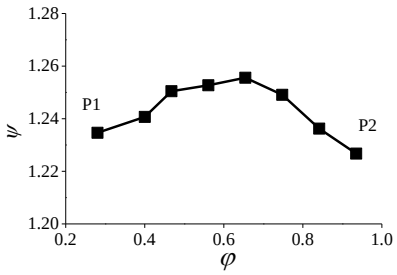

Figure 10. Performance curve by two-dimensional simulations

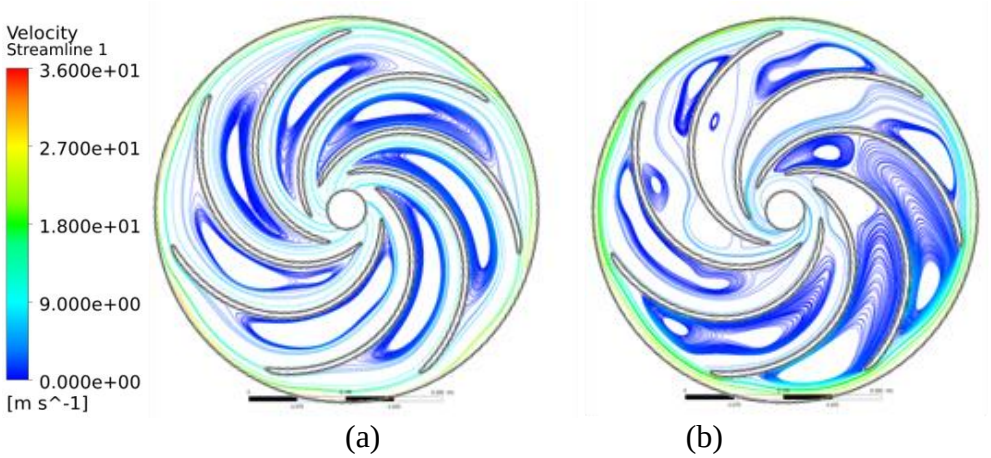

Figure 11. Streamlines in the impeller at (a) P1 and (b) P2

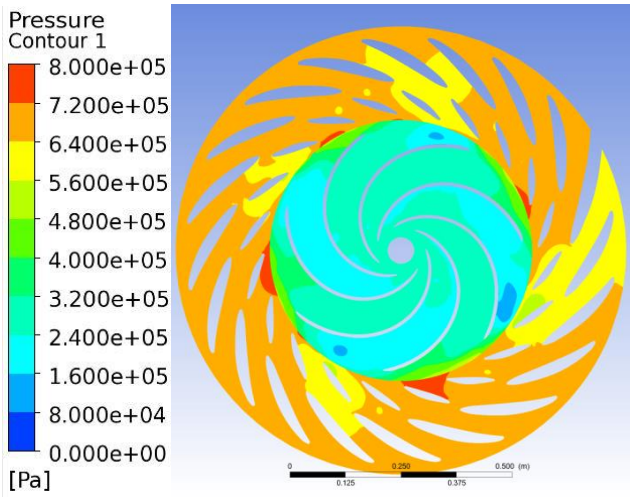

Figure 12. Pressure distribution in impeller, guide vane and stay vane channels at P1

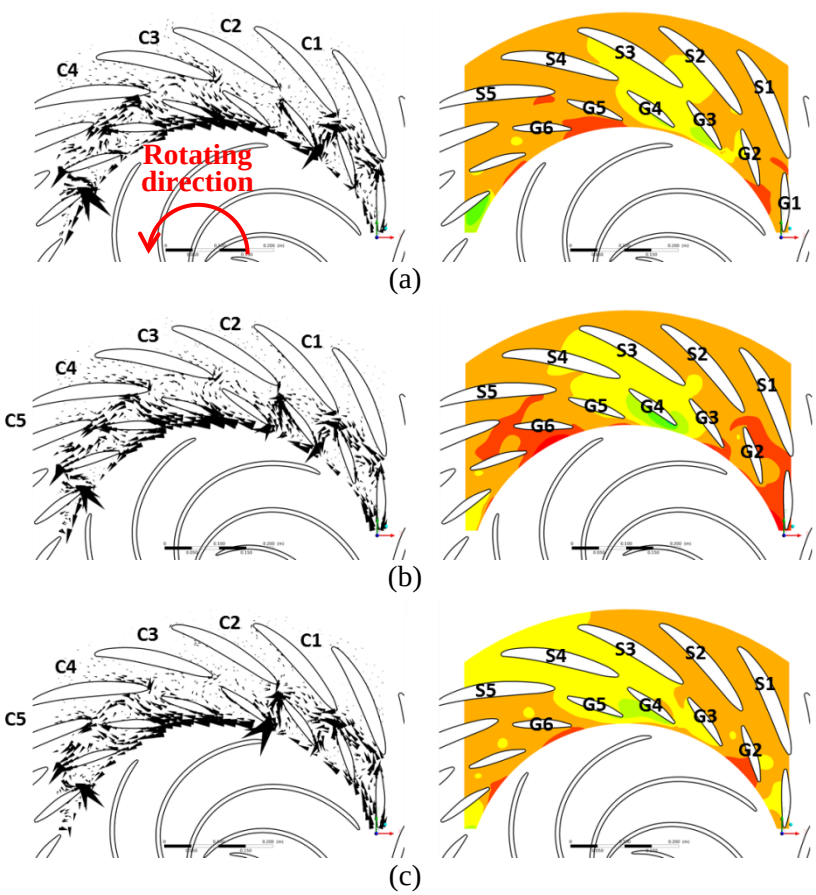

Figure 13. The distribution of velocity (left) and pressure (right)

in guide and stay vane at (a) t=0, (b) $t=\frac{1}{30}T$ and (c) $t=\frac{1}{15}T$

6. Concluding remarks

A low specific speed pump-turbine was experimentally and numerically investigated in the present study. The conclusions were drawn as follows:

- The positive slope region was detected on each GVO curve except at the optimum GVO. The positive slope occurs in the discharge coefficient between 80%-85% optimum discharge coefficient at every GVO.
- Hysteresis was detected by comparing the pump performance curves between measurements with increasing and decreasing discharge coefficients at three different GVOs (α=145%, 75% and 45%). The positive slope occurs at a smaller discharge coefficient when decreasing the discharge coefficient.
- The measurements of the pressure coefficient fluctuations in the draft tube, vaneless space and the stay vane channel atα=45% were applied with decreasing the discharge coefficient. The dominant frequency of pressure fluctuations is the BPF at large discharge coefficient. The occurrence of rotating stall with two cells was also proven when the discharge coefficient decreases into the positive slope region, by confirming the occurrence of a low-frequency fluctuation and cross phase analysis.
- Two-dimensional simulation was applied for a further understanding to the flow mechanism of the rotating stall. The positive slope on the performance curve was detected in the results of the two-dimensional simulations. Four high pressure regions and low pressure regions (cells) distribute alternately in circumferential and rotate along the rotating direction of impeller at the condition with positive slope, indicating the occurrence of the rotating stall.

Acknowledgments
The authors would like to thank the Chinese National Foundation of Natural Science (No. 51476083) for its financial supports.

Nomenclatures

D: impeller inlet diameter (m)
ρ: density (kg/m3)
p: pressure (Pa)
Q: discharge (m3/s)
H: head (m)
t: time (s)
b: width of impeller outlet (m)
n: rotating speed of impeller (r/min)
u_2:circumferential velocity at impeller outlet (m/s)
α: relative guide vane opening
f: frequency
f_n: rotating frequency
n_q: specific speed, $n_q = \frac{n\sqrt{Q}}{H^{0.75}}$
φ: discharge coefficient, $\varphi = \frac{Q}{nD^3}$
ψ: energy coefficient, $\psi = \frac{gH}{n^2D^2}$
C_p: pressure coefficient, $C_p = \frac{p}{\frac{1}{2}\rho u_2^2}$

Subscripts:

min: minimum value in the positive slope region
max: maximum value in the positive slope region
2D: two-dimensional

References

[1] Yang C.J. Pumped hydroelectric storage, invited submission to Wiley Encyclopedia of Energy, John Wiley & Sons, Hoboken, NJ.
[2] Rau N.S. The state of energy storage in electric utility systems and its effect on renewable energy resources, NREL/TP-462-5337, UC Category:1371, DE94006947.
[3] Gülich JF. Centrifugal pumps. Berlin: Springer, 2008.
[4] Braun O. Part load flow in radial centrifugal pumps. École Polytechnique Fédérale de Lausanne, 2009.
[5] Pacot O. Large scale computation of the rotating stall in a pump-turbine using an overset finite element large eddy simulation numerical code. École Polytechnique Fédérale de Lausanne, 2014.
[6] Eisele K, Muggli F, Zhang Z, Casey M, Sallaberger M. Experimental and numerical studies of flow instabilities in pump-turbine stages. XIX IAHR Symposium, Singapore. 1998.
[7] Braun O, Kueny JL, Avellan F. Numerical analysis of flow phenomena related to the unstable energy-discharge characteristic of a pump-turbine in pump mode. ASME 2005 Fluids Engineering Division Summer Meeting. American Society of Mechanical Engineers, 2005.
[8] IEC60193, Hydraulic turbines, storage pumps and pump turbines-model acceptance tests; 1999.
[9] Sun Y, Zuo Z, Liu S, Liu J, Wu Y. Distribution of pressure fluctuations in a prototype pump turbine at pump mode. Advances in Mechanical Engineering 6 (2014): 923937.
[10] Sano T, Yoshida Y, Tsujimoto Y, Nakamura Y, Matsushima T. Numerical study of rotating stall in a pump vaned diffuser. Journal of fluids engineering 124.2 (2002): 363-370.